Electrodeposited Nanoporous versus Nanoparticulate ZnO Films of Similar Roughness for Dye-Sensitized Solar Cell Applications

V. M. Guerin,[†] C. Magne,[‡] Th. Pauporté,*[,†] T. Le Bahers,[†] and J. Rathousky[§]

Laboratoire d'Électrochimie, Chimie des Interfaces et Modélisation pour l'Énergie, UMR7575, CNRS-Chimie Paristech, ENSCP, 11 rue P. et M. Curie, 75231 Paris cedex 05, France, Saint-Gobain Recherche, 39 quai Lucien Lefranc, 93303 Aubervilliers Cedex France, and J. Heyrovsky Institute of Physical Chemistry, Academy of Sciences of the Czech Republic, Dolejskova 3, 18223 Prague 8, Czech Republic

ABSTRACT We present a comparative study of two different ZnO porous film morphologies for dye-sensitized solar cell (DSSC) fabrications. Nanoparticulate ZnO was prepared by the doctor-blade technique starting from a paste containing ZnO nanoparticles. Nanoporous ZnO films were grown by a soft template-assisted electrochemical growth technique. The film thicknesses were adjusted at similar roughness of about 300 in order to permit a worthy comparison. The effects on the cell performances of sensitization by dyes belonging to three different families, namely, xanthene (eosin Y) and indoline (D102, D131, D149 and D205) organic dyes as well as a ruthenium polypyridine complex (N719), have been investigated. The mesoporous electrodeposited matrix exhibits significant morphological changes upon the photoanode preparation, especially upon the dye sensitization, that yield to a dramatic change of the inner layer morphology and increase in the layer internal specific surface area. In the case of indoline dyes, better efficiencies were found with the electrodeposited ZnO porous matrixes compared to the nanoparticulate ones, in spite of significantly shorter electron lifetimes measured by impedance spectroscopy. The observation is interpreted in terms of much shorter transfer time in the oxide in the case of the electrodeposited ZnO films. Among the tested dyes, the D149 and D205 indoline organic dyes with a strong acceptor group were found the most efficient with the best cell over 4.6% of overall conversion efficiency.

KEYWORDS: ZnO • dye-sensitized solar cells • electrodeposition • nanoporous layer • nanoparticles • impedance spectroscopy

1. INTRODUCTION

Semiconductor oxides are key materials for photovoltaic applications, especially in the fields of organic−inorganic hybrid and dye-sensitized solar cells (DSSCs) (1−4). These devices aim at drastically lowering the production costs and promoting large-scale solar energy conversion. To date, the most successful DSSCs have been produced using porous TiO_2 nanocrystalline films combined with ruthenium polypyridine complex dyes (3, 4). However, ZnO has recently emerged as a promising alternative semiconductor material to TiO_2 with marked performance improvements of ZnO-based DSSCs achieved during the past few years (2, 5−12). ZnO is a n-type semiconductor combining a large bandgap of 3.37 eV at room temperature and an electron affinity similar to that of TiO_2 (13). The dynamic of the electron transfer process between the classical dyes and ZnO has been found in the subpicosecond range, a value comparable to the dye-TiO_2 systems (14). Moreover, single-crystalline ZnO exhibits a good electron transport collection and a fast charge transfer due to an electron mobility and a diffusion coefficient significantly higher than in the case of TiO_2 (2). Among the specific advantages of ZnO, one can cite the facility to grow elongated and single-crystalline hexagonal ZnO nanocrystals for the facile electron transport between the excited dye and the back contact with reduced recombination losses (15, 16). ZnO nanostructures and hierarchical structures are also on the basis of fruitful new concepts for DSSCs such as light scattering aggregates (6, 12, 17).

During the past decade, an impressive variety of ZnO nanostructures have been synthesized, assembled as thin films by various growth methods. Among them, electrochemical deposition and chemical bath deposition show characteristics advantageous for forming films with a high internal roughness. Electrochemical deposition is a simple and low-cost route for the preparation of nanoporous films possessing a large surface area (9, 18−23). It involves electronic charge exchange upon deposition, and this ensures an excellent electrical contact between the deposited oxide layer and the substrate at the origin of an excellent charge transfer at the back contact in the case of DSSCs. Moreover, ZnO electrodeposition is performed at low temperatures and in soft environments compatible with lightweight plastic flexible and other fragile substrates (24). The

* To whom correspondence should be addressed. E-mail: thierry-pauporte@chimie-paristech.fr.
Received for review September 2, 2010 and accepted November 4, 2010
[†] CNRS-Chimie Paristech.
[‡] Saint-Gobain Recherche.
[§] Academy of Sciences of the Czech Republic.
DOI: 10.1021/am1008248

as-deposited material is well-crystallized without requiring a postgrowth high temperature thermal treatment for crystallization or sintering. High surface area mesoporous ZnO films can be electrodeposited using an organic dye as an additive. The dye is a complexing compound for zinc ions dissolved in the solution and acts as a structure directing agent (7, 25). The architecture of the deposited ZnO nanostructure has been described as governed by the dye which is included and self-organized in the ZnO layer upon deposition (7, 25). It results in the formation of a hybrid organic/inorganic film. The dye can be subsequently removed by a soft treatment, and then, a mesoporous film is obtained that can be sensitized for solar cell applications (19, 26, 27).

In the present work, ZnO-based DSSCs prepared using nanoparticulate films and nanoporous electrodeposited ZnO films made of large single crystalline grains have been compared. The former were prepared by the classical doctor-blade technique starting from a paste containing ZnO nanoparticles. The latter were grown by the dye-assisted electrochemical growth technique described by Yoshida and colleagues (26). Films of similar roughness have been used in order to permit a worthy comparison, and various dyes have been investigated. It is shown that the mesoporous electrodeposited matrix exhibits significant morphological changes upon preparation, especially upon sensitization, that conduct to a dramatic increase in the layer internal specific surface area. Different organic dyes have been tested, and the conjugated indoline dyes have been found more efficient than the N719 commercial ruthenium-based dye. The cell performances are impacted by the ZnO layer structure, and for instance, we have observed that, for indoline dyes, the overall conversion efficiencies are better with the electrodeposited ZnO in spite of an electron lifetime, measured by impedance spectroscopy, significantly shorter than in the case of the nanoparticulate matrix.

2. EXPERIMENTAL SECTION

2.1. Porous Thin Film Synthesis. Porous films of ZnO were prepared on F-doped SnO_2 transparent electrodes (FTO) by dye-assisted electrodeposition and by sol−gel techniques. The substrates were carefully cleaned with soap and rinsed with deionized water prior to being sonicated for 5 min in ethanol, 5 min in acetone, and then 2 min in concentrated 45% HNO_3. In the case of the nanoparticulate films, the FTO substrate was finally heated at 450 °C during 30 min in a furnace.

The nanoparticulate films (hereafter designated as *np*-ZnO) were prepared by the doctor-blade technique. One gram of commercial ZnO nanoparticles (Degussa VP) was mixed in 5 g of ethanol, with 0.28 g of ethyl cellulose (5-15), 0.20 g of ethyl cellulose (30-70), and 4 g of terpineol to create a viscous solution. The mixture was sonicated, and ethanol was then removed in a rotary-evaporator to create a paste. The ZnO paste was doctor-bladed upon the FTO coated glass substrate to give a film with a thickness of 12 to 13 μm once dried. The dried films were placed in a tubular furnace and heated 30 min at 410 °C. The optimized heating temperature was determined by measuring cell performances for annealing temperatures ranging between 350 and 450 °C (Figure S1, Supporting Information). The ZnO electrodeposition was performed in a bath composed of 5 mM $ZnCl_2$ (Merck), 0.1 KCl (Fluka), and 50 μM eosin Y (EY; Kento). It was saturated with molecular oxygen by gas bubbling. The substrate was fixed to a rotating electrode and rotated at 300 rpm upon deposition. The applied potential was −1 V vs SCE (saturated calomel electrode), and the deposition time was adjusted to reach the desired film thickness. A zinc wire was used as a counter electrode. The as-deposited hybrid films were transparent but turned red-colored after exposure to air due to the oxidation at air of the dye present in the film (25). Eosin Y incorporated within the film was subsequently removed by soaking in a KOH solution at pH 10.5 during 3 h, according to a procedure described by Yoshida and colleagues (26, 20). In the following, the electrodeposited ZnO films are designated as *ed*-ZnO.

Table 1. Porous Properties of *np*-ZnO Films and of *ed*-ZnO Films upon Preparation Determined by Profilometry, BET, and SEM Characterizations[a]

film	thickness/ μm	R_{BET}/ $cm^2 \cdot cm^2$	S_{BET}/ $m^2 \cdot cm^{-3}$	pores size/ nm
np-ZnO	12	300	23	∼60
As-grown ZnO/EY	2	∼1−2	∼0	nonporous
ed-ZnO after desorption	2	56	28	∼10
ed-ZnO readsorbed with EY	2	125	62	<8

[a] R_{BET}: film roughness; S_{BET}: specific surface area reported to the film volume.

2.2. Film Characterization. The film thicknesses were measured with a Dektak 6 M stylus profiler. The sample morphologies were examined with a high resolution Ultra 55 Zeiss FEG scanning electron microscope (SEM) at an acceleration voltage of 10 kV. X-ray diffraction spectra were recorded with a Siemens D5000 apparatus operated at 40 kV and 45 mA using the Cu Kα radiation with $\lambda = 1.5406$ Å and a rotating sample holder. The accessible geometric surface area of films with a diameter of 20 mm was determined from adsorption isotherms of Kr at the boiling point of liquid nitrogen (approximately 77 K) using an ASAP 2010 apparatus (Micromeritics). The molecular area of krypton was taken as 0.21 nm^2 as recommended by the equipment producer. Prior to each adsorption measurement, the samples were outgassed at 150 °C overnight.

2.3. Solar Cell Fabrication. Solar cells were fabricated using films with a thickness of about 12 and 4.8 μm for *np*-ZnO and *ed*-ZnO, respectively. In both case, we did not observe significant efficiency enhancement with thicker ZnO layers. From BET (Brunauer, Emmett and Teller) results, the two types of films had a similar internal roughness, defined as the effective surface area over the projected area, of about 300 (Table 1). The films were dried at 150 °C during 1 h. Upon cooling, they were immersed in the dye solution. Dyes of different families were evaluated for ZnO cell sensitization: a xanthene dye, eosin Y (EY; Kento), the classical ruthenium polypyridine complex denoted N719 (Dyesol), and a series of indoline dyes, namely D102, D131, D149, and D205 (Chemicrea, Inc.; see the Supporting Information, Figure S2). For each dye, the optimized sensitization time was determined by preparing the cells and measuring their performances. This parameter was found dependent on the chemical nature of the dye. For EY, the ZnO matrixes were immersed 1 h in a 0.5 mM dye ethanolic solution at 60 °C. The N719 dye was dissolved in ethanol at 0.5 mM (5). Indoline dyes were prepared in a 1:1 mixture of acetonitrile/*tert*-butanol at 0.5 mM. The impregnation time was 2 h for the former dye and 1 h for the latter dyes. The counter electrode was prepared by spreading a H_2PtCl_6 solution on a FTO/glass substrate and heating at 385 °C for 30 min. The final Pt loading was 5 $nM \cdot cm^{-2}$ (28). The liquid electrolyte was composed of 0.6 M tetrabutylamonium iodide (Sigma), 0.1 M LiI (Fluka), and 0.05 M I_2 (Aldrich) in acetonitrile. TBP (terbutylpyridine; 0.5 mM) was added in the case of N719 dye. This additive was

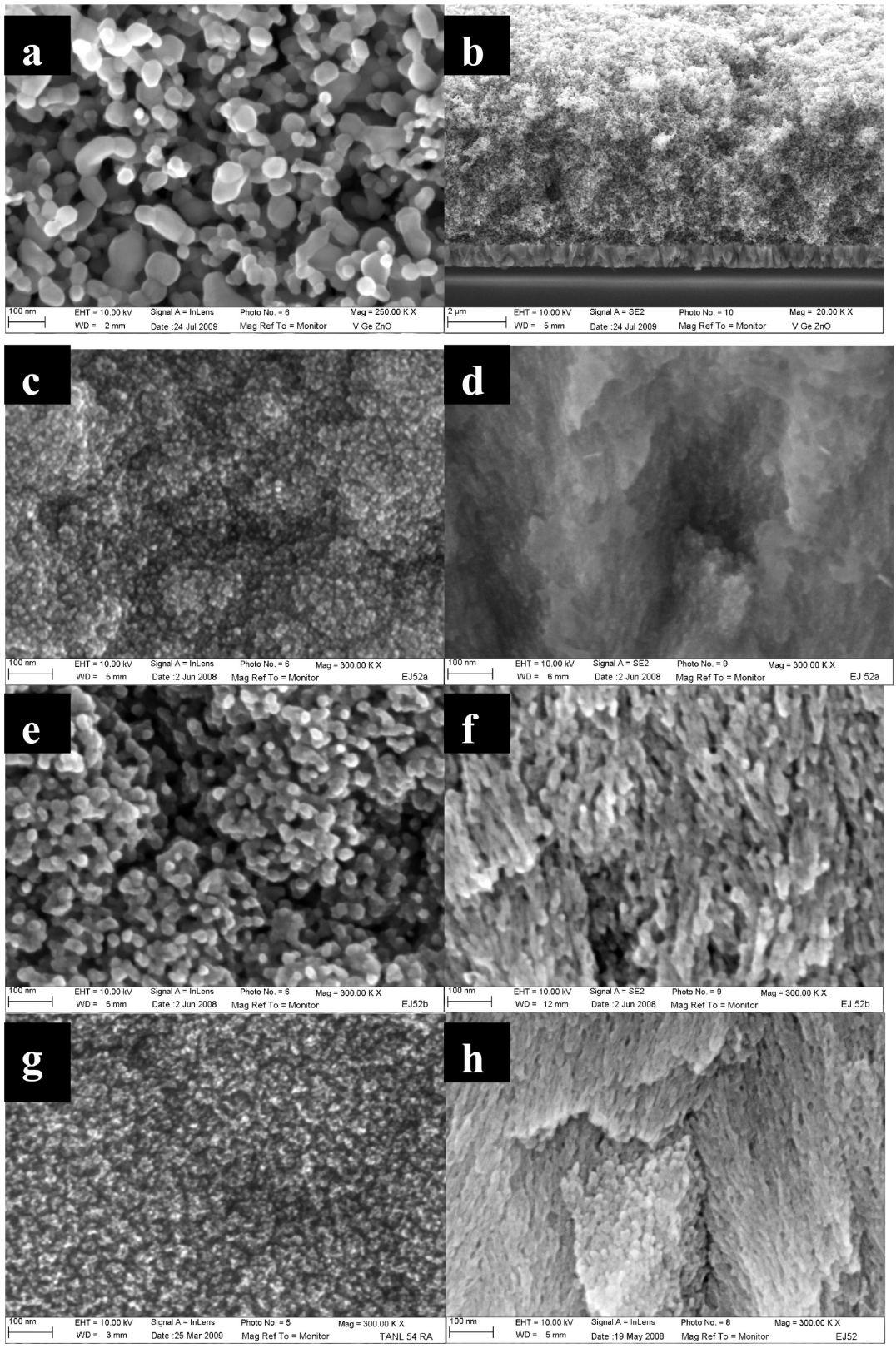

FIGURE 1. (a,b) SEM views of a *np*-ZnO film. (c−h) Morphological changes upon *ed*-ZnO film preparation: (c,d) As-electrodeposited film; (e,f) After EY structure directing agent removing; (g−h) After EY dye readsorption. (left) Top views; (right) side views.

avoided in the case of the organic dyes since we have shown recently that if, on the one hand, TBP increases slightly the V_{oc} of the cell, it also desorbs the sensitizer and then it deteriorates the solar cell performances rapidly with time (29). In the case of the optimized D149 cell, the electrolyte composition was 0.05 I_2 and 0.5 M 1-2,dimethyl,3-propylimidazolium iodide in acetonitrile. The active area of the cells was 0.25 cm^2 except for the optimized cell for which a 0.07 cm^2 dark mask was used. The cell was illuminated by a solar simulator (Abet Technology sun 2000) equipped with an AM 1.5 global filter. The energy density was calibrated with a silicon reference cell and fixed at 100 mW/cm^2. The $J-V$ curves were recorded by a Keithley 2400 digital

sourcemeter using 0.01 V/s voltage ramp rate. The impedance spectra were measured at the open circuit voltage under 1 sun AM 1.5 illumination by a Solartron FRA1255 coupled with a PAR 283 potentiostat. The AC signal was 10 mV, and the frequency range was 100 kHz−0.1 Hz. The spectra were simulated with the Z-view software from Scribner Associates.

3. RESULTS AND DISCUSSION

3.1. Porous ZnO Thin Films' Preparation and Properties. Figure 1a,b is high resolution SEM images of the nanoparticulate films. The films were porous with an open structure and large pores with a diameter of about 60 nm. The structure was stable, and no significant morphological change could be observed after the layer sensitization. XRD was used to follow the crystallinity of the layer upon film preparation (Figure S3, Supporting Information). The Scherrer's formula gave an estimate of the mean particle size upon the film preparation process (30). The initial value in the powder was 25 and 29 nm in the paste dried at 150 °C after doctor blading. After the thermal treatment at 410 °C, the typical size dimension increased at 53 nm due to the film sintering which gave rise to the ZnO nanoparticle merging as observed on the SEM view of Figure 1a.

The morphological changes that occurred upon the *ed*-ZnO mesoporous film preparation were also investigated by SEM. Figure 1c−h shows the layer morphology upon the successive stages of the photoanode preparation. The starting as-grown film was dense, and no voids could be observed even on zoomed views (Figure 1c,d). After the eosin Y extraction in a mild alkaline solution, the pores were released, showing that they were initially almost fully filled by the EY dye (Figure 1e,f) (20, 26, 31). The pores were formed upon the electroprecipitation of ZnO around elongated EY aggregate structures that acted as a self-assembled template (7). In Figures 1f and S4 (Supporting Information), one can observe the presence of pores with a mean size of about 10 nm which are oriented perpendicular to the substrate. Previous investigations on epitaxial electrodeposited films have shown that the films are made of large porous single crystalline grains, with a length corresponding to the film thickness and a width of several hundred of nanometers (Figure S4, Supporting Information) (7, 21). However, an interesting observation of the present work is that the film structure was changed again upon the dye readsorption step. After adsorption of EY (Figure 1g,h), the pores became finer and distributed in a denser manner. Their main diameter on the micrograph was about 7 to 8 nm. The SEM observations suggest an in-deep reorganization upon the dye adsorption step, even if the initial ZnO porous film was dried at 150 °C before the dye readsorption step. This singular reorganization is probably due to a reactive role of the dye solution that must favor the dissolution/precipitation of the oxide in organic solutions.

The porosity of the films was further investigated by the Kr adsorption experiments. Figure 2A shows the Kr isotherms at ca. 77 K which have been related to the film volume for the sake of correct comparison. The flat isotherm of *np*-ZnO (a) without any hysteresis loop corresponds to a

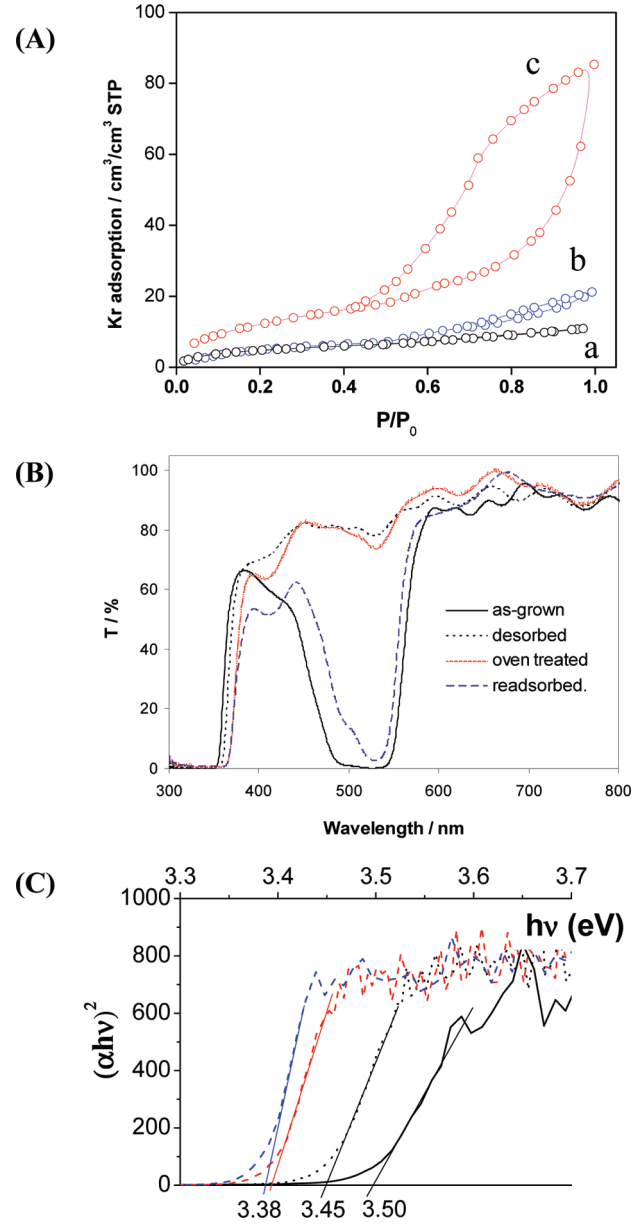

FIGURE 2. (A) BET adsorption isotherms of Kr at 77 K related to the film volume. (a) *np*-ZnO film prepared by the doctor-blade technique. (b,c) *ed*-ZnO at various stage of the photoanode preparation: (b) desorbed *ed*-film and (c) after readsorption with EY dye. (B) Specular transmission curves of the electrodeposited film upon photoanode preparation. (C) ZnO bangap determination upon preparation from the $(\alpha^* h\nu)^2 = f(h\nu)$ curves extracted from (B).

macroporous material, whose surface is practically flat regarding the Kr adsorption. The as-grown *ed*-ZnO/EY hybrid film (not shown) was nonporous, in agreement with its dense aspect on the SEM images. After dye desorption and the opening of the pores, the specific surface area related to the film's unit volume increased to 28 m^2/cm^3 (Table 1). As there is only a hint of the hysteresis loop, a vast majority of the pores was definitely larger than circa 10 nm. A dramatic change in the film's morphological properties occurred upon the eosin readsorption, shown by the change in the shape of the adsorption isotherms, especially by the creation of the large hysteresis loop (Figure 2B). The specific area related to the geometric film area and to the film total volume

Table 2. *I*−*V* Characteristics of Solar Cells Using *np*-ZnO Films Sensitized by a Xanthene Dye (EY), a Ru-Based Dye (N719), and a Series of Indoline Dyes (D205, D149, D102, and D131) under 100 mW·cm^{-2} Illumination, AM 1.5[a]

dye	η (%)	V_{oc} (V)	J_{sc} (mA·cm^{-2})	FF (%)
EY	1.69	0.65	3.66	70.9
N719	2.79	0.55	8.33	61.2
D205	3.08	0.58	9.87	53.9
D149	2.84	0.54	10.05	52.5
D102	1.89	0.54	6.27	55.9
D131	1.29	0.55	3.63	65.0

[a] η: overall conversion efficiency; V_{oc}: open circuit voltage; J_{sc}: short circuit current; FF: filling factor. The error is ±5%.

increased to 125 cm^2·cm^{-2} and 62 m^2·cm^{-3}, respectively. The large hysteresis loop is due to the filling by Kr of pores smaller than circa 8 nm. The films contained also some proportion of larger pores, as a horizontal plateau was not achieved at the relative pressure P/P_0 approaching 1. The dramatic increase in the specific surface area and the decrease in the pore size cannot be explained by the adsorption of a dye monolayer inside the pores. Therefore, there must have been an in-depth reorganization of the layer during the sensitization step. The same effect was also observed with other dyes such as D149. Another interesting remark is that the in-depth layer reorganization did not occur in the case of *np*-ZnO which is more stable probably due to the use of stable nanoparticulate building blocks and of high temperature for the film preparation.

Changes in the *ed*-ZnO layer upon photoanode preparation could also be followed by transmission measurements (Figure 2B). The as-grown ZnO/EY hybrid film was characterized by two features: a bandgap absorption edge in the UV and an absorption peak centered at 520 nm which is due to the red-colored EY dye. After the dye desorption and oven treatment, the absorption due to EY almost disappeared and the UV-absorption edge was red-shifted. The dye adsorption step was characterized by the reappearance of the dye absorption peak. The peak was less intense due to the formation of a dye self-assembled monolayer instead of aggregated dyes included in the layer. An interesting fact is the observed ZnO band-edge shift upon the film preparation. The bangap of ZnO (E_g) was estimated from the transmission curves (Figure 2C) and was found to be 3.50 eV for the as-grown film, 3.45 eV after dye desorption, and 3.38 eV after the oven treatment. The dye readsorption did not significantly change the E_g value. The E_g shift may be due to the presence of a zinc hydroxide phase in the initial layer (32). The treatment in the aqueous mild alkaline medium as well as the oven treatment probably eliminate that phase by dehydration and ZnO formation. The final E_g value is typical of ZnO (32).

3.2. ZnO-Based Dye-Sensitized Solar Cells. Dye-sensitized solar cells were prepared using *np*-ZnO and *ed*-ZnO films of similar roughness and sensitized by various dyes. The cell performances obtained in the case of *np*-ZnO are summarized in Table 2. The corresponding *I*−*V* polarization curves recorded under standard illumination conditions are reported in Figure 3. The best performances were found for the D205 indoline dye with an efficiency of 3.08%. The performances were higher than in the case of the classical N719 dye (2.79%). N719 dye has a much lower molar extinction coefficient than the organic dyes tested in the present study (14). This may in part explain the observed lower performances. Furthermore, the Ru dyes have been described as forming aggregates with Zn(II) for long sensitization time (33, 34). In the present case, the adsorption time was optimized but the presence of aggregates due to the acidic properties of the dye cannot be excluded. The lower performance of the EY-based DSSC is due to the rather sharp absorption peak of this pink-red colored dye. Only a reduced part of the visible light region was absorbed by the dye, explaining the rather low short-circuit current of the cells. The cells exhibited satisfactory V_{oc} and FF as well as low dark current. They can be explained by the well-covering of the ZnO surface in that case due to the limited size of the EY molecule (35).

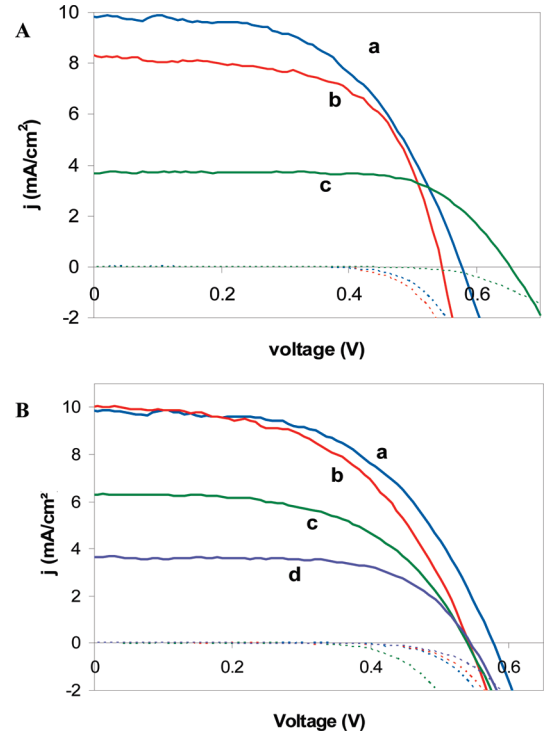

FIGURE 3. *I*−*V* curves under 1 sun AM 1.5 illumination and dark current of *np*-ZnO-based DSSCs sensitized by various dyes. (A): (a) D205; (b) N719; (c) EY. (B): (a) D205; (b) D149; (c) D102; (d) D131.

Indoline dyes are metal-free molecules that are interesting alternatives to conventional Ru-based dyes. High performances and stability have been shown in the case of TiO_2-based DSSCs (36, 37). A series of indoline sensitizers have been investigated here with the *np*-ZnO films. The results are shown in Figure 3b and Table 1. The performance order is η(D131) < η(D102) < η(D149) < η(D205), in good agreement with the results for TiO_2 nanoparticulate cells as reviewed in ref 13. The order for the three first dyes can be assigned to the progressive red-shift of the maximum of absorbance wavelength that renders the absorption spectrum more fitted to the solar spectrum (13). The redshift is

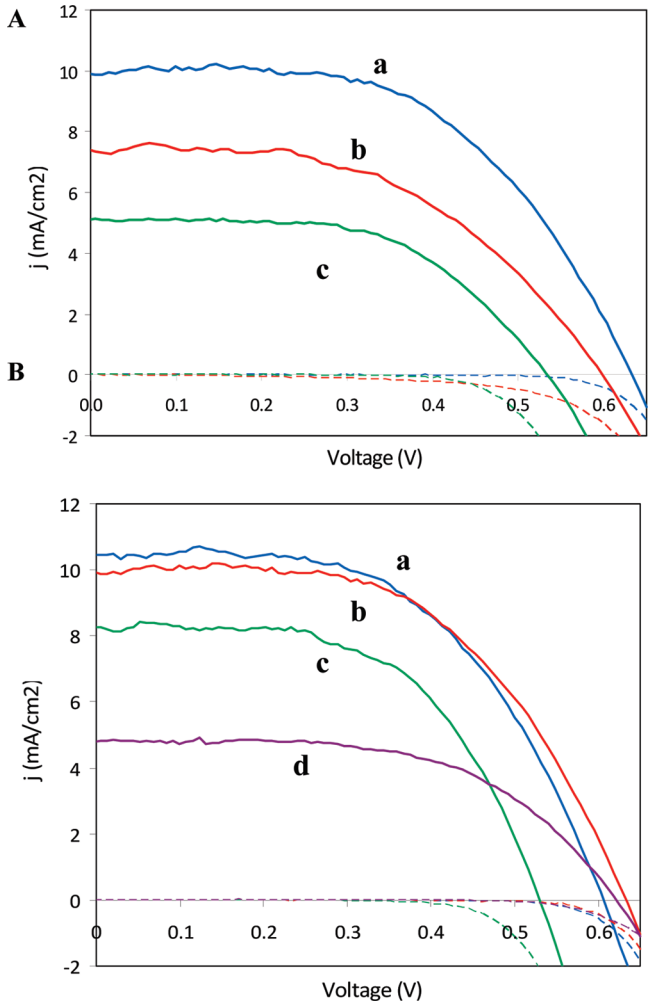

FIGURE 4. *I*−*V* curves under 1 sun AM 1.5 illumination and dark current of *ed*-ZnO-based DSSCs sensitized by various dyes. (A): (a) D149; (b) N719; (c) EY. (B): (a) D205; (b) D149; (c) D102; (d) D131.

due to the increase in the acceptor group strength (two bonded rhodanine groups in the case of D149 and D205) and then to the decrease in the lowest unoccupied molecular orbital (LUMO) energy level. The LUMO level has been demonstrated to remain superior to the ZnO conduction band level by recent density-functional theory (DFT) calculations (13). The D205 is an amphiphilic derivative of D149 in which the ethyl chain on a N of the terminal rhodanine ring is replaced by an octyl chain (see Figure S2, Supporting Information). The superior performances of this dye is due to the presence of the long alkyl chain which has been described to prevent the recapture of photoinjected electron by the triiodine ions within the electrolyte (37). It results mainly in a higher V_{oc} of the cells.

The *I*−*V* curves of cells prepared using the nanoporous *ed*-ZnO are presented in Figure 4, and the characteristics are summarized in Table 3. The performances of EY and N719 cells were similar for both ZnO matrixes. However, the *ed*-ZnO cells sensitized with indoline dyes exhibited higher efficiencies than the *np*-ZnO cells. The same *I*−*V* characteristics were found for D149 and D205 with an overall conversion efficiency of about 3.5%. It is worth mentioning that with the *ed*-ZnO the performance ranking order of the

Table 3. *I*−*V* Characteristics of Solar Cells of 0.25 cm^2 Using *ed*-ZnO Films Sensitized by a Xanthene Dye (EY), a Ru-Based Dye (N719), and a Series of Indoline Dyes (D205, D149, D102, and D131) under 100 mW·cm^{-2} Illumination, AM 1.5[a]

dye	η (%)	V_{oc} (V)	J_{sc} (mA/cm^{-2})	FF (%)
EY	1.57	0.53	5.1	57.6
N719	2.25	0.60	7.4	51.0
D205	3.45	0.60	10.4	54.7
D149	3.47	0.64	9.9	55.0
D102	2.53	0.53	8.2	57.8
D131	1.74	0.62	4.8	58.5
D149[b]	4.64	0.59	11.0	72.0

[a] The error is ±5%. [b] Optimized cell with $S = 0.07$ cm^2; see the text for details about cell optimizing.

indoline sensitized cells was the same as for *np*-ZnO: η(D131) < η(D102) < η(D149) ~ η(D205), with no beneficial effect of the long alkyl chain for the D205 dye. Compared to *np*-ZnO, the better performances of indoline sensitized *ed*-ZnO is due to higher V_{oc}. The higher V_{oc} is probably due to the lower thickness of the *ed*-ZnO layers. We can imagine that the absorption profile is different for the two kinds of films and that the electron density is higher in the thinner film. Since the position of the quasi-fermi level depends on the density of injected electrons (29), this parameter is significantly improved in the case of *ed*-ZnO and a better V_{oc} is found. This effect may be improved by the local increase in the triiodide concentration in the thinner ZnO films under illumination (see below).

To better understand the functioning of the cells, electrochemical impedance spectroscopy (EIS) measurements under one sun illumination were conducted. The spectra are presented in Figure 5 for the *np*-ZnO-based cells and in Figure 6 for the *ed*-ZnO-based cells. They were always characterized by two main relaxation loops which have been analyzed by means of the classical equivalent electrical circuit presented in Figure 5a (38, 39). Constant Phase Elements (CPE), with an electrical impedance written as $Z_{CPE} = 1/T(j\omega)^P$, were used instead of pure capacitances for a better fit. R_s is the resistance due to the contacts. The high frequency loop is classically assigned to the redox reaction at the charged counter-electrode, and the low-frequency loop is due to the injection−recombination reaction at the photoanode. The impedance contribution of the electron transport by diffusion in the photoanode was negligible in our case and masked by the counter-electrode impedance. The counter-electrode and the photoanode loops could be fitted to each other with a R//CPE circuit. We can note that the diffusion of tri-iodide in the acetonitrile electrolyte was a quick step in all our cells and that the corresponding low frequency impedance could be neglected, masked by the photoanode contribution.

In the case of the *np*-ZnO electrodes (Table 4), the P_2 parameter was close to 1 and the CPE was almost a pure capacitance. The lifetimes of the electrons (τ_e) in the photoanode were calculated from the low-frequency loop parameters of the spectra. The dispersion of capacitance was first

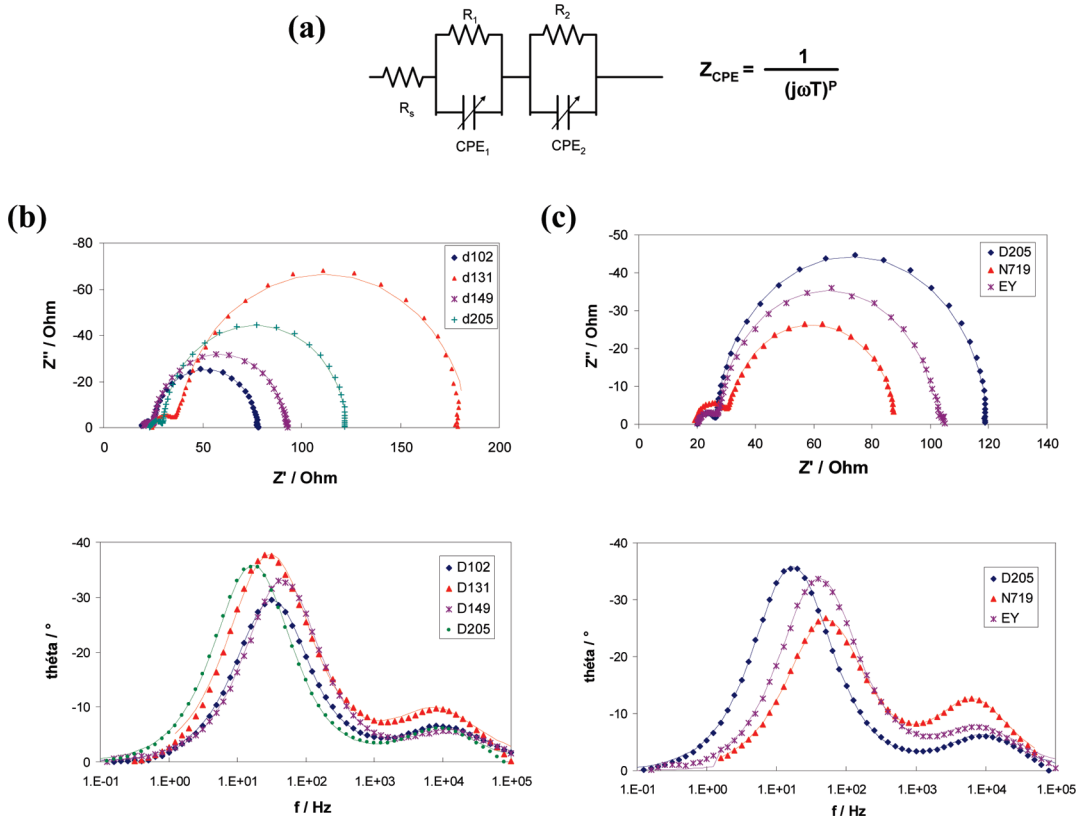

FIGURE 5. (a) Equivalent electrical circuit used to model the electrical behavior of the cells under illumination. (b,c) EIS spectra under 1 sun AM 1.5 of *np*-ZnO solar cells sensitized by (b) indoline dyes and (c) three families of dyes. (top) Nyquist plot; (bottom) phase versus the frequency. The points are the experimental data, and the lines are the fits.

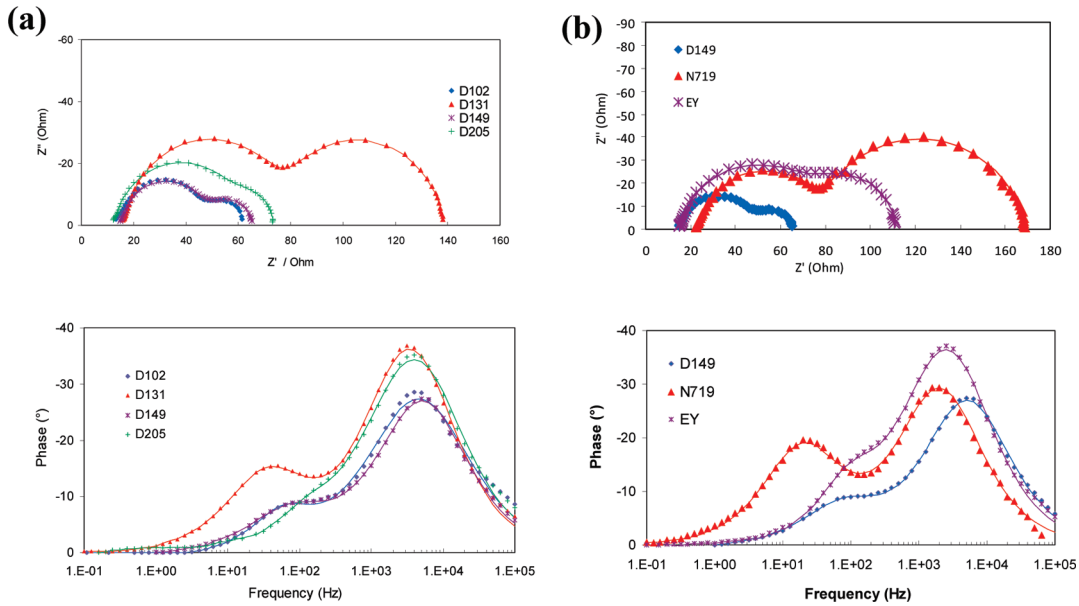

FIGURE 6. EIS spectra under 1 sun AM 1.5 of *ed*-ZnO solar cells sensitized by (a) indoline dyes and (b) three families of dyes. (top) Nyquist plot; (bottom) phase versus the frequency.

corrected according to a procedure described in the literature (40, 41) to obtain the corresponding capacitance:

$$C_2 = (R_2^{1-P2}T)^{1/P2}$$

and

$$\tau_e = 2\pi R_2 C_2$$

The values are summarized in Table 4. In the case of the *np*-ZnO films, they were ranged between 36 and 79 ms, except in the case of the D205 dye for which we have noticed a remarkably high value at 122 ms. The long electron lifetime for the D205 dye can be assigned to the lateral octyl

Table 4. Equivalent Circuit Parameters of *np*-ZnO-Based Solar Cells Sensitized with a Series of Dyes[a]

	R_s (Ω)	R_1 (Ω)	T_1 (× 10^6)	P_1	R_2 (Ω)	T_2 (× 10^5)	P_2	τ/ms
EY	19	7	14	0.86	75	13	0.96	50
N719	19	15	17	0.94	76	11	0.93	36
D205	21	6	6	0.94	93	24	0.97	122
D149	20	5	9.8	0.88	67	12	0.96	43
D102	19	6	17	0.84	53	19	0.97	56
D131	20	13	14	0.82	147	11	0.94	79

[a] Measurement at the V_{oc} under 1 sun AM 1.5. The error is ±2%.

Table 5. Equivalent Circuit Parameters of *ed*-ZnO-Based Solar Cells Sensitized with a Series of Dyes[a]

	R_s (Ω)	R_1 (Ω)	T_1 (× 10^6)	P_1	R_2 (Ω)	T_2 (× 10^5)	P_2	τ/ms
EY	16	61	7.5	0.88	35	6.2	0.99	13
N719	21	65	1.3	0.82	92	23	0.91	90
D205	16	49	7.8	0.86	13	11	1	20
D149	17	34	6.4	0.87	17	28	0.9	16
D102	16	38	12	0.81	11	17	1	28
D131	18	61	4.4	0.9	62	17	0.9	38

[a] Measurement at the V_{oc} under 1 sun AM 1.5. The error is ±2%.

chain on the terminal rhodanine ring that imparts the molecule with amphiphilic properties. The lateral chain improved the dye coverage of the surface and reduced the contact between the electrolyte and the ZnO surface. This significantly reduced recapture reaction between the injected electron and the tri-iodide ions in the electrolytic solution. This hypothesis is confirmed by a higher V_{oc} in the case of D205 compared to D149.

In Figure 6 are presented the EIS spectra of the cells fabricated using the *ed*-ZnO films. A detailed comparison of the fit parameters is presented in Table 5. The lifetime of the electron in the semiconductor was significantly reduced compared to the *np*-ZnO cells except for the N719 dye. They ranged between 13 and 38 ms (90 ms for N719). This could be attributed to two main reasons: (i) due to the lower thickness of the *ed*-ZnO film and the higher electron injection, the local concentration of tri-iodide in the pores must be high in the case of *ed*-ZnO and then accelerate the recapture rate. (ii) It can also be supposed that it must be rather difficult to obtain a very well self-organized organic dye covered ZnO surface when the pores of the SC are very small, as it is the case for *ed*-ZnO, even if we have a similar dye loading for the two kinds of films.

After N719, τ_e is the highest in the case of *ed*-ZnO sensitized with the D131 dye and this dye also gave rise to a rather high τ_e value in the case of *np*-ZnO films. D131 dye is the smallest of the investigated indoline dyes which may facilitate its penetration in the small pores of the *ed*-ZnO films and the surface coverage. τ_e is of the same order of magnitude for D149 and D205 dyes in *ed*-ZnO. There was no performance improvement here in the case of the amphiphilic D205 compound, and the two cells had similar overall conversion efficiencies. This surprising observation may be attributed to the large steric size of the molecule and its stacking tendency which may render the sensitization of the finely porous *ed*-ZnO more difficult compared to the *np*-ZnO films.

At first sight, the higher efficiency of the indoline system dyes in *ed*-ZnO cells with a shorter electron lifetime compared to *np*-ZnO cells may appear puzzling. However, the collection of the photogenerated electrons in DSSCs is a complicated process that results from a competition between (i) the electron transfer in the SC from the excited dye to the back contact and (ii) its recapture by the tri-iodide ions in solution (42, 43). High conversion efficiencies are achieved when the collection efficiency is high, that is when the transfer time is much shorter than the electron lifetime. In the case of *ed*-ZnO, the charge transfer between the excited dye and the back contact is very fast due to a film thickness reduced by a factor of 2.5 and to a large single crystalline structure of the ZnO nanoporous grains. The latter property has been clearly shown for instance in the case of epitaxial nanoporous *ed*-ZnO films (21). On the contrary, it is well-known that the electron transfer is slowed-down in the case of the nanoparticulate films prepared by sol−gel techniques (44, 45). This is due to the presence of a high concentration of traps at the numerous grain boundaries between the nanoparticles. The present comparative experiments emphasize the utmost importance of the oxide quality for ZnO cell performances and the interest of the use of large single-crystalline phases for achieving fast charge collection. They also illustrate the difficulty of sensitizing finely nanoporous ZnO photoanodes with classical high efficiency dyes with a large steric size.

In the light of the above-described work, the *ed*-ZnO/D149 system appeared as the most interesting and we have concentrated our efforts to gain in efficiency by optimizing various parameters of this cell (see Experimental Section). The matrix was sensitized by a mixture of D149 and cholic acid according to the procedure described in ref 27 to avoid the formation of dye aggregates. LiI and tetrabutylamonium iodide were replaced by 1-2,dimethyl,3-propylimidazolium iodide, and a mask was used to define the cell surface area. The performance of the best cell is presented in Table 3 and Figure S5 (Supporting Information). If the V_{oc} was slightly decreased due to the use of a mask and then the increase of the dark current density, the fill factor reached a very satisfactory value of 0.72 and the short circuit current was slightly improved at 11 $mA \cdot cm^{-2}$, giving an overall conversion efficiency of 4.64%. The electron lifetime was measured at 27 ms.

4. CONCLUSIONS

The design of ZnO porous films is an important challenge to improve the light collection by the dye sensitizer and charge collection at the back contact of the DSSC photoanodes. In the present work, by comparing two different ZnO porous layers of similar roughness but prepared by two different growth methods, important information has been collected that should be helpful for optimizing the system. We have shown the advantage of preparing highly crystalline ZnO film to increase the cell efficiency even if the electron

lifetime, measured by impedance spectroscopy, is not as high as in the nanoparticulate films. However, in future works, it will be important to increase the V_{oc} of the ZnO cells to get a higher efficiency. If the conduction band energy level of ZnO is higher than the TiO_2 one, this theoretical advantage to reach a high V_{oc} is not found in our experimental work and in the literature data. The local confinement of tri-iodide in the finely nanoporous *ed*-ZnO electrode improves the V_{oc} but is detrimental for the electron lifetime. It will be also important to increase the light absorption by the dyes to achieve a high short circuit current in these cells. The N719 dye has not been found well-adapted to the sensitizing of *ed*-ZnO films due to a low molar extinction coefficient, a large steric size, and its acidity that render the oxide sensitization difficult. The sensitization of ZnO with organic dye seems more promising even if the ideal dye is not available yet and will require a lot of work to be found. In the present work, the best results have been obtained with an indoline dye which has given a maximum overall conversion efficiency over 4.6%.

Acknowledgment. Dr. H. Miura (Chemicrea Inc., Japan) is acknowledged for kindly providing us with the indoline dyes. The authors are grateful to Prof. P. Barboux (LCMCP, ChimieParistech, France) for his help in nanoparticulate thin film preparation by doctor blade. We acknowledge Saint Gobain Recherche (Aubervilliers, France) for its support. The French National Agency of Research (ANR) is thanked for financial support by means of the Asyscol supported project (ANR-08-HABISOL-002). Th.P acknowledges the CNRS for financial support in the framework of the PIE-program (nanoZnO-solar PR08-2.1-10).

Supporting Information Available: Optimized *nc*-ZnO film heating treatment. Molecular structure of the investigated sensitizers. XRD of the nanoparticulate films upon layer preparation. Cross-sectional SEM view of an *ed*-ZnO film after EY desorption. Characteristics of the optimized cell. This material is available free of charge via the Internet at http://pubs.acs.org.

REFERENCES AND NOTES

(1) Oosterhout, S. D.; Wienk, M. M.; Van Bavel, S. S.; Thiedmann, R.; Koster, L. J. A.; Gilot, J.; Loos, J.; Schmidt, V.; Janssen, R. A. J. *Nat. Mater.* **2009**, *8*, 818.
(2) Zhang, Q.; Dandeneau, C. S.; Zhou, X.; Cao, G. *Adv. Mater.* **2009**, *21*, 4087.
(3) O'Regan, B.; Grätzel, M. *Nature* **1991**, *353*, 737.
(4) Nazeeruddin, M. K.; De Angelis, F.; Fantacci, S.; Selloni, A.; Viscardi, G.; Liska, P.; Ito, S.; Takeru, B.; Gratzel, M. G. *J. Am. Chem. Soc.* **2005**, *127*, 16835.
(5) Keis, K.; Magnusson, E.; Lindström, H.; Lindquist, S. E.; Hegfeldt, A. *Sol. Energy Mater. Sol. Cells* **2002**, *73*, 51.
(6) Zhang, Q.; Chou, T. P.; Russo, B.; Jenekhe, S. A.; Cao, G. *Angew. Chem., Int. Ed.* **2008**, *47*, 2402.
(7) Yoshida, T.; Minoura, H.; Zhang, J.; Komatsu, D.; Sawatani, S.; Pauporté, T.; Lincot, D.; Oekermann, T.; Schlettwein, D.; Tada, H.; Wohrle, D.; Funabiki, K.; Matsui, M.; Miura, H.; Yanagi, H. *Adv. Funct. Mater.* **2009**, *19*, 17.
(8) Chen, Z. G.; Tang, Y. W.; Zhang, L. S.; Luo, L. J. *Electrochim. Acta* **2006**, *51*, 5870.
(9) Saito, M.; Fujihara, S. *Energy Environ. Sci.* **2008**, *1*, 280.
(10) Zhang, Q.; Dandeneau, C. S.; Zhou, X.; Cao, G. *Adv. Mater.* **2009**, *21*, 4087.
(11) Gonzalez-Valls, I.; Lira-Cantu, M. *Energy Environ. Science* **2009**, *2*, 19.
(12) Cheng, H. M.; Hsieh, W. F. *Energy Environ. Sci.* **2010**, *3*, 442.
(13) Le Bahers, T.; Pauporté, T.; Scalmani, G.; Adamo, C.; Ciofini, I. *Phys. Chem. Chem. Phys.* **2009**, *11*, 11276.
(14) Bauer, C.; Boschloo, G.; Mukhtar, E.; Hagfeldt, A. *J. Phys. Chem. B* **2001**, *105*, 5585.
(15) Law, M.; Greene, L. E.; Johnson, J. C.; Saykally, R.; Yang, P. *Nat. Mater.* **2005**, *4*, 455.
(16) Lupan, O.; Guérin, V. M.; Tiginyanu, I. M.; Ursaki, V. V.; Chow, L.; Heinrich, H.; Pauporté, T. *J. Photochem. Photobiol. A* **2010**, *211*, 65.
(17) Xu, C. K.; Shin, P.; Cao, L. L.; Gao, D. *J. Phys. Chem. C* **2010**, *114*, 125.
(18) Pauporté, T.; Yoshida, T.; Cortès, R.; Froment, M.; Lincot, D. *J. Phys. Chem. B* **2003**, *107*, 10077.
(19) Yoshida, T.; Pauporté, T.; Lincot, D.; Oekermann, T.; Minoura, H. *J. Electrochem. Soc.* **2003**, *150*, C608.
(20) Pauporté, T.; Rathousky, J. *J. Phys. Chem. C* **2007**, *111*, 7639.
(21) Pauporté, T.; Yoshida, T.; Cortès, R.; Froment, M.; Lincot, D. *J. Phys. Chem. B* **2003**, *107*, 10077.
(22) Goux, A.; Pauporté, T.; Yoshida, T.; Lincot, D. *Langmuir* **2006**, *22*, 10545.
(23) Graaf, H.; Maedler, C.; Kehr, M.; Oekermann, T. *J. Phys. Chem. C* **2009**, *113*, 6910.
(24) Lupan, O.; Pauporté, T. *J. Cryst. Growth* **2010**, *312*, 2454.
(25) Goux, A.; Pauporté, T.; Lincot, D.; Dunsch, L. *ChemPhysChem* **2007**, *8*, 926.
(26) Yoshida, T.; Iwaya, M.; Ando, H.; Oekermann, T.; Nonomura, K.; Schlettwein, D.; Wöhrle, D.; Minura, H. *Chem. Commun.* **2004**, *4*, 400.
(27) Dentani, T.; Kubota, Y.; Funabiki, K.; Jin, J.; Yoshida, T.; Minoura, H.; Miura, H.; Matsui, M. *New J. Chem.* **2009**, *33*, 93.
(28) Hasin, P.; Alpuche-Aviles, M. A.; Li, Y.; Wu, Y. *J. Phys. Chem. C* **2009**, *113*, 7456.
(29) Le Bahers, T.; Labat, F.; Pauporté, T.; Ciofini, I. *Phys. Chem. Chem. Phys.* **2010**, *12*, 14710.
(30) Goux, A.; Pauporté, T.; Chivot, J.; Lincot, D. *Electrochim. Acta* **2005**, *50*, 2239.
(31) Graaf, H.; Maedler, C.; Kehr, M.; Oekermann, T. *J. Phys. Chem. C* **2009**, *113*, 6910.
(32) Pauporté, T.; Lincot, D. *Electrochim. Acta* **2000**, *45*, 3345.
(33) Keis, K.; Lindgren, J.; Lindquist, S. E.; Hagfeldt, A. *Langmuir* **2000**, *16*, 4688.
(34) Horiuchi, H.; Katoh, R.; Hara, K.; Yanagida, M.; Murata, S.; Arakawa, H.; Tachiya, M. *J. Phys. Chem. B* **2003**, *107*, 2570.
(35) Labat, F.; Ciofini, I.; Hratchian, H. P.; Frisch, M.; Raghavachari, K.; Adamo, C. *J. Am. Chem. Soc.* **2009**, *131*, 14290.
(36) Horiuchi, T.; Miura, H.; Uchida, S. *Chem. Commun.* **2003**, *24*, 3036.
(37) Ito, S.; Zakeeruddin, M.; Humpry-Baker, R.; Liska, P.; Charvet, R.; Comte, P.; Nazeeruddin, M.; Péchy, P.; Takata, M.; Miura, H.; Uchida, S.; Grätzel, M. *Adv. Mater.* **2006**, *18*, 1202.
(38) Bisquert, J.; Vikhrenko, V. S. *J. Phys. Chem. B* **2004**, *108*, 2313.
(39) Wang, Q.; Moser, J. E.; Grätzel, M. *J. Phys. Chem. B* **2005**, *109*, 14945.
(40) Brug, G. J.; Van den Eeden, A. L. G.; Sluyters-Rehbach, M.; Sluyters, J. H. *J. Electroanal. Chem.* **1984**, *176*, 275.
(41) Pauporté, T.; Finne, J. *J. Appl. Electrochem.* **2006**, *36*, 33.
(42) Oekermann, T.; Yoshida, T.; Minoura, H.; Wijayantha, K. G. U.; Peter, L. M. *J. Phys. Chem. B* **2004**, *108*, 8364.
(43) Nonomura, K.; Komatsu, D.; Yoshida, T.; Minoura, H.; Schlettwein, D. *Phys. Chem. Chem. Phys.* **2007**, *9*, 1843.
(44) Kalyanasundaram, K., Ed. *Dye-sensitized solar cells*; EPFL press: Lausanne, 2010; p331.
(45) Hagfeldt, A.; Boschloo, G.; Sun, L.; Kloo, L.; Pettersson, H. *Chem. Rev.* **2010**, *110*, 6595.

AM1008248